Memoirs of the Faculty of Engineering, Okayama University, Vol.31, No. 1, pp.19-33, December 1996

# *Structure of Dusty Plasma as Yukawa System Confined in One-Dimensional External Fields*

Hiroo Totsuji*, Tokunari Kishimoto*, and Chieko Totsuji*

(Received October 18 , 1996)


## SYNOPSIS

As a model of dusty plasmas in external fields, Yukawa system in a one-dimensional external field is analyzed by molecular dynamics simulations and theoretical approaches. It is shown that particles form clear thin layers (sheets) at low temperatures and the number of layers changes discretely with characteristic parameters of the system, accompanying the rearrangements of whole system from nearly equipartitioned layers to also nearly equipartitioned layers. The number, positions and populations of layers are obtained as functions of characteristic parameters. The shell (sheet) model which has been successful for confined one-component plasmas is extended to this system and results of numerical experiments are reproduced to a good accuracy. The effect of cohesive energy in each layer is of essential importance to reproduce discrete changes in the number of sheets.


## 1 INTRODUCTION

Dusty plasma is an ensemble of charged macroscopic particles or particulates suspended in environmental plasmas composed of microscopic particles. The behavior of dusty plasmas has recently attracted much interest from the viewpoints of both plasma applications and basic plasma physics. Dust particles are often observed in plasma processes in semiconductor engineering and they are closely related to the quality of the products of such processes. On the other hand, particulates are artificially introduced into these plasmas and formation of dust crystals has been observed.[1, 2, 3, 4] Since the size, the density, and the temperature of these particulates are easy to observe and control, such dusty systems are expected to be one of ideal materials for experiments on classical fluids and solids.[5] The purpose of this paper is to make numerical experiments on the behavior of dusty plasma and give a theoretical model which reproduces the results of numerical experiments to a good accuracy.

In Section 2, our model of dusty plasma in external fields is presented and its characteristic parameters are defined. In Section 3, the methods and the results of numerical experiments are given. A theoretical model is analyzed and its predictions are compared with the results of numerical experiments in Section 4 and conclusions are given in Section 5. Some details of numerical methods and theoretical approaches are given in Appendices A and B.

*Department of Electrical and Electronic Engineering

# 2 A MODEL OF DUSTY PLASMA: YUKAWA SYSTEM IN ONE-DIMENSIONAL EXTERNAL FIELDS

## 2.1 Interaction Potential

The interaction potential between macroscopic particles depends on both their own physical parameters and those of surrounding plasmas. There may exist various possibilities for these parameters and accordingly for the interaction potential. In order to understand the behavior of dusty plasma in complex conditions, however, the results for the simple and basic case are indispensable. As such a case, we assume that macroscopic particles are interacting via the isotropic Yukawa potential[7]

$$v(r) = \frac{q^2}{r}\exp(-\kappa r). \tag{1}$$

Here $q$ is the charge which is assumed to be the same for all particles, $r$, the distance, and $1/\kappa$, the screening length. Yukawa system has been extensively investigated as a simple system which smoothly interpolates classical systems with short-range and long-range interactions and as a model of charge stabilized colloidal suspensions.[8] These works, however, have been mainly on the uniform system with infinite extensions.

## 2.2 External Potential

In addition to mutual interactions, macroscopic particles are under the effect of various external forces such as gravitation, electrostatic force, ion drug, and so on. There may be again many possibilities for these force fields. As in the case of mutual interaction, we may take the simplest case to obtain basic understanding of the behavior of macroscopic particles and assume that the total effect of external forces is expressed by an extenal potential

$$v_{ext}(z) = \frac{k}{2}z^2. \tag{2}$$

We expect that the uniformity in the other two directions may be satisfied around the center of experimental apparatus and the parabolic form may simulate the total potential near the equilibrium plane $z = 0$.

## 2.3 Characteristic Parameters

The classical system of particles with the interaction (1) at thermal equilibrium with the temperature $T$ is characterized by two independent dimensionless parameters. With appropriately defined mean distance $a$, these parameters may be given by

$$\Gamma = \frac{q^2}{ak_BT}, \tag{3}$$

and

$$\xi = \kappa a. \tag{4}$$

In the limit $\kappa \to 0$ (or $\xi \to 0$), $\Gamma$ reduces to the usual parameter for the one-component plasma (OCP) which designates the ratio of the average interaction potential to thermal energy. In our case with finite values of $\xi$, the latter ratio is approximately given by $\Gamma\exp(-\xi)$ rather than $\Gamma$.

In the external field (2), we have another independent dimensionless parameter which is related to the ratio of the external potential to thermal energy. We may thus take

$$\frac{ka^2}{k_BT} \tag{5}$$

as such a parameter. Since our system is confined by a force along the $z$-direction, the mean distance may be defined by

$$N_s = \frac{1}{\pi a^2}, \tag{6}$$

where $N_s$ is the surface number density in the $xy$-plane.

In this paper, we are mainly concerned with the structure of dust particles at low temperatures. In this case, both $\Gamma$ and (5) diverge and only their ratio has physical meaning. We adopt $\xi$ and

$$\eta = \frac{\pi^{1/2}}{4}\frac{ka^2/k_BT}{q^2/ak_BT} = \frac{k}{4\pi q^2 N_S^{3/2}} \tag{7}$$

as two independent dimensionless parameters at low temperatures. The extra factor is added for the sake of consistency with the case of OCP.[9, 10]

# 3 NUMERICAL EXPERIMENTS

## 3.1 Molecular Dynamics

### 3.1.1 Deformable Periodic Boundary Conditions

In order to simulate the Yukawa system with infinite extensions in $x$ and $y$ directions, we impose the periodic boundary conditions along these directions in our molecular dynamics. Noting that the shape of the periodicity sometimes strongly influences the distribution, especially its symmetry, of particles, we take into account the deformation of fundamental vectors of periodicity. In the case of OCP, it has been explicitly shown that the relaxation of the Coulomb lattice to the correct symmetry is only possible with deformations of periodic boundaries.[11]

We express the coordinates of particles $\mathbf{r}$ by

$$\mathbf{r} = \mathbf{R} + z\hat{z} = \mathsf{h}\cdot\mathbf{X} + z\hat{z}. \tag{8}$$

Here $\hat{z}$ is the unit vector in the $z$-direction, $\mathbf{R}$ is a vector in the $xy$-plane, and $\mathsf{h}$ is a $2\times 2$ tensor composed of fundamental (column) vectors of periodicity $\mathbf{a}$ and $\mathbf{b}$ as

$$\mathsf{h} = (\mathbf{a}, \mathbf{b}). \tag{9}$$

The deformation of $\mathbf{a}$ and $\mathbf{b}$ is taken into account by the Lagrangian[12]

$$\mathcal{L}_0(\{\mathbf{X}_i, z_i, \dot{\mathbf{X}}_i, \dot{z}_i\}, \mathsf{h}, \dot{\mathsf{h}}) = \sum_i \frac{m}{2}(\dot{\mathbf{X}}_i\cdot\mathsf{G}\cdot\dot{\mathbf{X}}_i + \dot{z}_i\dot{z}_i) - U(\mathsf{h}, \{\mathbf{X}_i, z_i\}) + \frac{W}{2}\mathrm{Tr}\left[\dot{\mathsf{h}}^t\cdot\dot{\mathsf{h}}\right]. \tag{10}$$

Here dots denote time derivatives,

$$\mathsf{G} = \mathsf{h}^t\cdot\mathsf{h}, \tag{11}$$

$U$ is the interaction energy, and $W$ is the effective mass for the motion of fundamental vectors. Though in principle the value of $W$ does not affect the results so far as one follows the dynamics for a sufficiently long time, it needs to be optimized in practice. We have adoped $W/m \sim 10$ in our simulations.

The equations of motion are given by

$$m\frac{d}{dt}\mathsf{G}\cdot\frac{d}{dt}\mathbf{X}_i = -\frac{\partial}{\partial\mathbf{X}_i}U, \tag{12}$$

$$m\frac{d^2}{dt^2}z_i = -\frac{\partial}{\partial z_i}U, \tag{13}$$

and

$$W\frac{d^2}{dt^2}\mathsf{h} = (\mathsf{K}+\Pi)\cdot\sigma. \tag{14}$$

Here

$$\sigma = (\mathsf{h}^{-1})^t \det\mathsf{h}, \tag{15}$$

and $\mathsf{K}$ and $\Pi$ are defined by

$$\mathsf{K} = \frac{1}{\det\mathsf{h}}\sum_i m\left(\mathsf{h}\cdot\dot{\mathbf{X}}_i\right)\left(\mathsf{h}\cdot\dot{\mathbf{X}}_i\right) \tag{16}$$

and

$$\Pi_{\alpha\beta} = -\frac{1}{\det\mathsf{h}}\sum_\gamma \frac{\partial U}{\partial h_{\alpha\gamma}}h_{\beta\gamma}, \tag{17}$$

respectively. Ewald type method is applied to the calculation of $U$ and $\Pi$. Details are given in Appendix A.

### 3.1.2 Dynamics at Constant Volume

In order to perform simulations with given values of surface number density in the $xy$-plane, we add a term

$$-p_{ext}\det\mathsf{h} \tag{18}$$

to $\mathcal{L}_0$. Eq. (14) is then modified into the form

$$W\frac{d^2}{dt^2}\mathsf{h} = (\mathsf{K}+\Pi-p_{ext}\mathsf{1})\cdot\sigma \tag{19}$$

and the conservation of the Hamiltonian is written as

$$\frac{d}{dt}(\mathcal{H}_0 + p_{ext}\det\mathsf{h}) = \det\mathsf{h}\frac{dp_{ext}}{dt} \tag{20}$$

where $\mathcal{H}_0$ is the Hamiltonian for $\mathcal{L}_0$.

We determine the Lagrange multiplier (the pressure in the $xy$-plane) $p_{ext}(t)$ by the condition that the area of the unit cell $\det\mathsf{h}$ is kept constant. This condition reduces to[11]

$$p_{ext}(t) = \frac{\mathrm{Tr}(\sigma^t\cdot\Pi\cdot\sigma) - (W/\det\mathsf{h})\mathrm{Tr}(\sigma^t\cdot\dot{\mathsf{h}}\cdot\sigma^t\cdot\dot{\mathsf{h}})}{\mathrm{Tr}(\sigma^t\cdot\sigma)}. \tag{21}$$

(Alternatively, we may simulate our system under given external pressure in the $xy$-plane by keeping $p_{ext}$ constant in the course of time development.)

### 3.1.3 Dynamics at Constant Temperature

In order to simulate the canonical ensemble at the temperature $T$, we introduce a variable $s$ and the virtual time $t'$ by

$$dt = \frac{dt'}{s} \tag{22}$$

and consider the dynamics of a virtual system[13, 14] whose Lagrangian $\mathcal{L}'$ is given by

$$\mathcal{L}'(\{\mathbf{X}'_i, z'_i, \dot{\mathbf{X}}'_i, \dot{z}'_i\}, \mathsf{h}', \dot{\mathsf{h}}', s', \dot{s}', t') = \sum_i \frac{m}{2}s'^2(\dot{\mathbf{X}}'_i\cdot\mathsf{G}'\cdot\dot{\mathbf{X}}'_i + \dot{z}'_i\cdot\dot{z}'_i) - U(\mathsf{h}', \{\mathbf{X}'_i, z'_i\})$$
$$+\frac{W}{2}s'^2\mathrm{Tr}\left[\dot{\mathsf{h}}'^t\cdot\dot{\mathsf{h}}'\right] - p_{ext}(t')\det\mathsf{h}' + \frac{Q}{2}\dot{s}'^2 - gk_BT\ln s'. \tag{23}$$

Here we denote physical quantities of the virtual system by primes, $\cdot = d/dt'$, and $Q$ is the mass related to the heat reservoir.

Momenta in the virtual system are defined by

$$\Xi_i' = ms'^2 \mathsf{G}' \cdot \dot{\mathbf{X}}_i', \tag{24}$$

$$\zeta_i' = ms'^2 \dot{z}_i', \tag{25}$$

$$\mu' = Ws'^2 \dot{\mathsf{h}}', \tag{26}$$

$$p_s' = Q\dot{s}', \tag{27}$$

and the Hamiltonian of the virtual system is given by

$$\mathcal{H}'(\{\Xi_i', \zeta_i', \mathbf{X}_i', z_i'\}, \mathsf{h}', \mu', s', p_s', t') = \sum_i \frac{1}{2ms'^2}((\mathsf{G}'^{-1} \cdot \Xi_i') \cdot \Xi_i' + \zeta_i'\zeta_i') + U(\mathsf{h}', \{\mathbf{X}_i', z_i'\})$$
$$+ \frac{1}{2Ws'^2}\mathrm{Tr}\left[\mu'^t \cdot \mu'\right] + p_{ext}(t') \det \mathsf{h}' + \frac{1}{2Q}(p_s')^2 + gk_BT \ln s'. \tag{28}$$

The equations of motion for the virtual system are given by, all primes being omitted,

$$m\frac{d}{dt}s^2\mathsf{G} \cdot \frac{d}{dt}\mathbf{X}_i = -\frac{\partial}{\partial \mathbf{X}_i}U, \tag{29}$$

$$m\frac{d}{dt}s^2\frac{d}{dt}z_i = -\frac{\partial}{\partial z_i}U, \tag{30}$$

$$W\frac{d}{dt}s^2\frac{d}{dt}\mathsf{h} = (s^2\mathsf{K} + \Pi - p_{ext}\mathbf{1}) \cdot \sigma, \tag{31}$$

and

$$Qs\frac{d^2}{dt^2}s = \sum_i ms^2(\dot{\mathbf{X}}_i \cdot \mathsf{G} \cdot \dot{\mathbf{X}}_i + \dot{z}_i \cdot \dot{z}_i) + Ws^2\mathrm{Tr}\left[\dot{\mathsf{h}}^t \cdot \dot{\mathsf{h}}\right] - gk_BT. \tag{32}$$

The real variables and virtual variables are related as $s = s', \mathbf{X}_i = \mathbf{X}_i', z_i = z_i', \mathsf{h} = \mathsf{h}'$, and

$$\frac{d}{dt}s = s\frac{d}{dt'}s', \ \frac{d}{dt}\mathbf{X}_i = s\frac{d}{dt'}\mathbf{X}_i', \ \frac{d}{dt}z_i = s\frac{d}{dt'}z_i', \ \frac{d}{dt}\mathsf{h} = s\frac{d}{dt'}\mathsf{h}'. \tag{33}$$

The equations of motion in real variables are

$$m\frac{d}{dt}\mathsf{G} \cdot \frac{d}{dt}\mathbf{X}_i = -\frac{\partial}{\partial \mathbf{X}_i}U - m\frac{d\ln s}{dt}\mathsf{G} \cdot \frac{d}{dt}\mathbf{X}_i, \tag{34}$$

$$m\frac{d^2}{dt^2}z_i = -\frac{\partial}{\partial z_i}U - m\frac{d\ln s}{dt}\frac{d}{dt}z_i, \tag{35}$$

$$W\frac{d^2}{dt^2}\mathsf{h} = (\mathsf{K} + \Pi - p_{ext}\mathbf{1}) \cdot \sigma - W\frac{d\ln s}{dt}\frac{d}{dt}\mathsf{h}, \tag{36}$$

and

$$\frac{Q}{s}\frac{d^2}{dt^2}s = \sum_i m(\dot{\mathbf{X}}_i \cdot \mathsf{G} \cdot \dot{\mathbf{X}}_i + \dot{z}_i \cdot \dot{z}_i) + W\mathrm{Tr}\left[\dot{\mathsf{h}}^t \cdot \dot{\mathsf{h}}\right] - gk_BT + \frac{Q}{s^2}\left(\frac{ds}{dt}\right)^2. \tag{37}$$

As in the case of W, the value of $Q$ is arbitrary and to be optimized for practical purposes. In our simulations, we have taken $Q/mL^2 \sim 0.01$, where $L$ is the system size in $xy$-plane. According to whether the time average is taken over the virtual time $t'$ or the real time $t$, we set the parameter $g$ to be equal to $3N + (4-1) + 1$ or $3N + (4-1)$, $N$ and (4-1) being the number of particles in the unit cell and the number of freedom in $\mathsf{h}$, respectively.

## 3.2 Results of Simulation

### 3.2.1 Formation of Layers and Number of Layers as a Function of Parameters

Molecular dynamics simulations formulated above have been performed mainly with 1024 independent particles. We start from a state of sufficiently high temperature where particles form a cloud around the plane $z = 0$ and slowly reduce the temperature. With the decrease of the temperature, microscopic structures appear in the cloud. At sufficiently low temperatures, particles organize themselves into well-defined thin layers.[6] The behavior of the cloud at different temperatures and some examples of layered structures are shown in Fig. 1.

The number of layers $\mathcal{N}$ depends on the parameters of our system. Since such structures are observed at low temperatures, $\mathcal{N}$ is a function of two parameters of our system at low temperatures, $\xi$ and $\eta$; $\mathcal{N} = \mathcal{N}(\xi, \eta)$. Values of the function $\mathcal{N}(\xi, \eta)$ is shown in Fig. 2. In Fig. 3, we also plot the thickness of our system along $z$ as a function of these two parameters.

Let us first follow the behavior of $\mathcal{N}$ with a given value of $\xi$. The external potential $v_{ext}(z)$ tries to confine particles in the plane $z = 0$. In the limit of strong confining force or large values of the parameter $\eta$, particles are thus forced to be in the plane $z = 0$ and $\mathcal{N}(\xi, \eta \to \infty) = 1$. Mutual repulsions between particles, on the other hand, tend to increase the thickness, since mutual distances between particles increase with the increase of the thickness. Therefore, the thickness of particle distribution increases when the relative strength of the confining force $\eta$ becomes smaller. We here note that, as is shown in Fig. 2, this tendency appears as the increase of the number of layers occuring in very narrow ranges of the parameter $\eta$. In Fig. 3, we also observe that, when $\eta$ decreases, the thickness increases with discontinuities corresponding to the stepwise changes in $\mathcal{N}$.

The number of layers and the thickness along $z$ are thus determined as a result of the competition between the external confining force and mutual repulsion. When the parameter $\xi$ increases, mutual repusion becomes weaker and the number of layers increases for fixed value of the parameter $\eta$.

In the limit of small screening constant or $\xi \to 0$, our system reduces to the OCP. In this case, it has been shown both experimentally and theoretically that a confined finite system forms thin layers in accordance with the geometry of confinement at low enough temperatures, and the number of layers and the total thickness change discretely with the system parameter.[9, 10] Our results for the Yukawa system indicate that these properties are common for Coulomb and Coulomb-like systems. The results for OCP are consistent with our results for finite values of $\xi$.

### 3.2.2 Position and Population of Layers and Intra-Layer Symmetry

The position and population of each layer are shown in Figs. 4 and 5. Some examples of the distribution of particles in each layer are shown in Fig. 6.

In the case of OCP, the spacings and populations for all layers are almost equal and the spacings increase with the decrease of the parameter $\eta$.[15, 16] In the case of Yukawa system, the spacings and populations are also nearly equal just after the appearance of a new layer. With further decrease of the parameter $\eta$, however, the populations of outer layers become smaller and the spacings of outer layers become relatively smaller, all the spacings being expanded. Their values become almost equal again when another new layer appears.

Along with the decrease of the parameter $\eta$ in the range between the appearance of a new layer and that of another new layer, the symmetry of distribution of particles in each layer also repeats alternative changes from that of the square lattice to the triangular lattice. Some examples can be seen in Fig. 6. The relation between the inter-layer distance and intra-layer symmetry is shown in Fig. 7. This kind of transitions may be analogous to the case of OCP[17] and colloidal suspensions confined between glass plates,[18] where systematic changes of the symmetry with an increase or

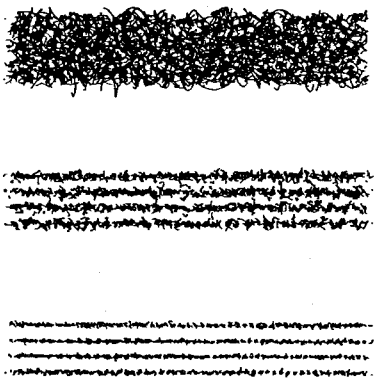

Fig. 1. Orbits; $\xi = 1$ and $\Gamma = 100$(top), 1000(middle), and 3000(bottom).

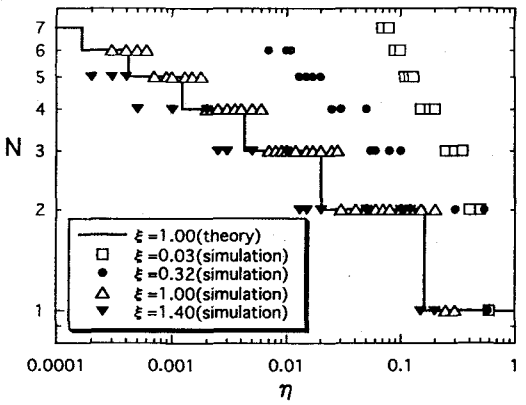


Fig. 2. Number of layers $\mathcal{N}$.

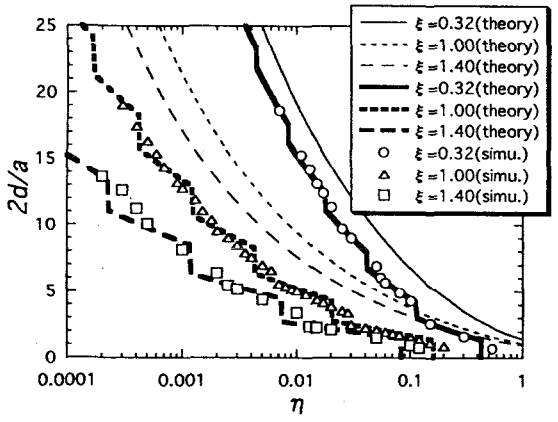


Fig. 3. Total thickness $2d$.

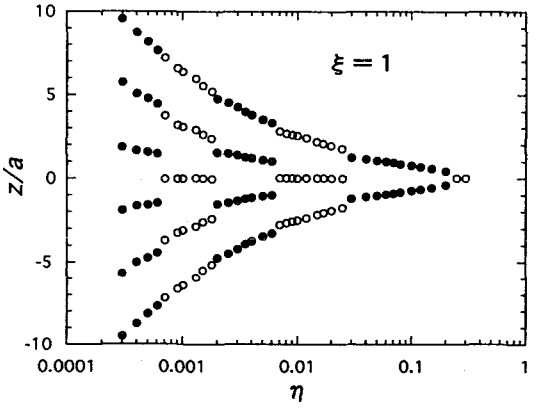


Fig. 4. Positions of layers $z_i$.

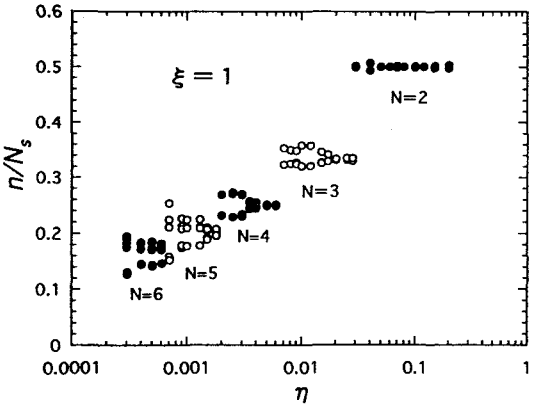


Fig. 5. Populations of layers $n_i/N_s$.

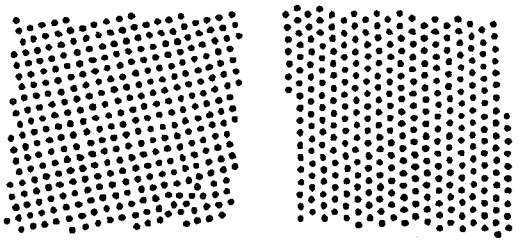

Fig. 6. Examples of distribution in layers.

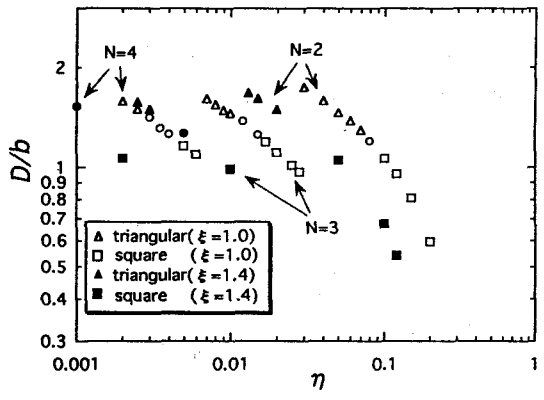


Fig. 7. Intra-layer symmetry vs. inter-layer distance $D$, $b$ being mean distance defined for each layer.

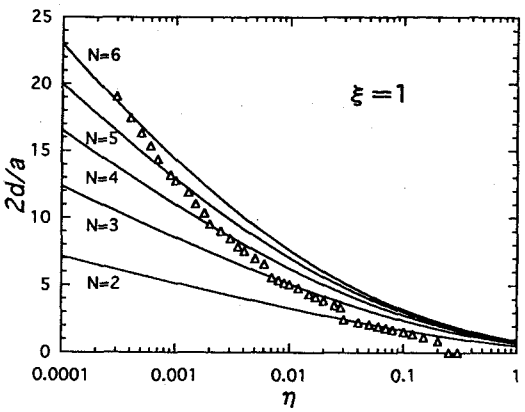


Fig. 8. Total thickness $2d$ given by (6).

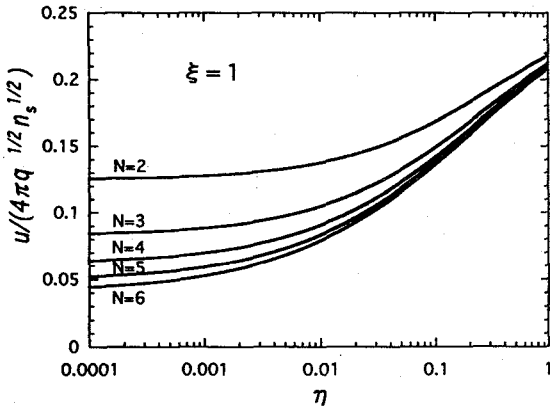


Fig. 9. Total potential energy $u$ given by (6).

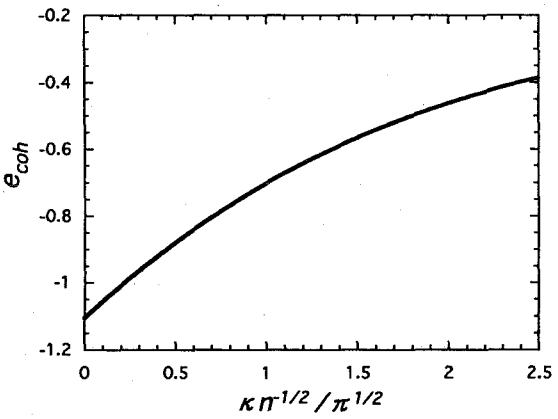


Fig. 10. Cohesive energy of triangular Yukawa lattice.

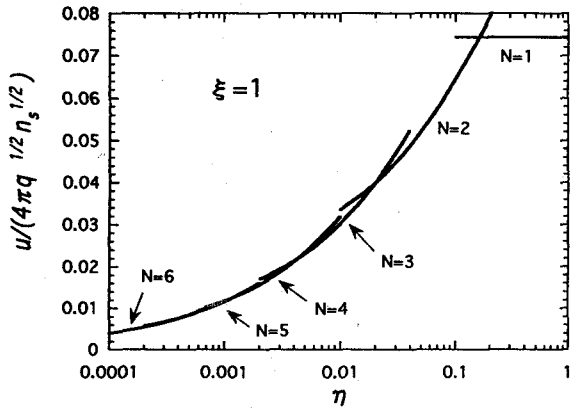


Fig. 11. Total potential energy $u$ given by (7).

decrease of the number of layers have been observed.

# 4 THEORETICAL ANALYSES BASED ON SHEET (SHELL) MODEL

## 4.1 Continuum Model: Estimation of Thickness

When particles are distributed uniformly in the domain $|z| < d$ with the surface number density $N_s$, the interaction energy is calculated as

$$\begin{aligned} &\frac{1}{2}\int\int d\mathbf{r}d\mathbf{r}'\frac{q^2}{|\mathbf{r}-\mathbf{r}'|}\exp(-\kappa|\mathbf{r}-\mathbf{r}'|)\left(\frac{N_s}{2d}\right)^2 \\ &= N_s\int d\mathbf{R}\frac{\pi}{2}\frac{q^2N_s}{\kappa^3d^2}[\exp(-2\kappa d)-1+2\kappa d]. \end{aligned} \tag{38}$$

Here $d\mathbf{R}$ denotes the surface element in the $xy$-plane and the integrand on the right-hand side is the interaction energy per particle. In the one-dimensional potential field $v_{ext}(z) = kz^2/2$, the total potential energy per particle of the uniform distribution with thickness $2d$ is thus given by

$$\frac{1}{6}kd^2 + \frac{\pi}{2}\frac{q^2N_s}{\kappa^3d^2}[\exp(-2\kappa d)-1+2\kappa d]. \tag{39}$$

The thickness of our system may be estimated by the value of $2d$ which minimizes this expression. When $\kappa = 0$, the thickness is given by

$$2d_0 = \frac{4\pi q^2N_s}{k}. \tag{40}$$

This result expresses that the confining potential $kz^2/2$ is equivalent to the existence of the background of opposite charges with the density $-k/4\pi q$.

With $d_0$, (39) is rewritten into the form

$$\frac{1}{6}kd^2\left\{1+\frac{3}{2}(\kappa d_0)^{-3}(d/d_0)^{-4}[\exp(-2(\kappa d_0)(d/d_0))-1+2(\kappa d_0)(d/d_0)]\right\}. \tag{41}$$

When $\kappa d_0 \ll 1$, the thickness is given by

$$\frac{d}{d_0} \sim 1-\kappa d_0, \tag{42}$$

and when $\kappa d_0 \gg 1$,

$$\left(\frac{d}{d_0}\right)^3 \sim \frac{3}{2}(\kappa d_0)^{-2}\{1+\exp[-2^{2/3}3^{1/3}(\kappa d_0)^{1/3}]\} - \left(\frac{3}{2}\right)^{2/3}(\kappa d_0)^{-7/3}. \tag{43}$$

In Fig. 3, optimum values of $2d/a$ are shown by thin lines and compared with results of numerical experiments.

For small values of $\xi$, especially for $\xi = 0$, our results for $2d/a$ are in good agreement with those of numerical experiments. For finite values of $\xi$, however, theoretical values of $2d/a$ largely overestimate experimental ones. In this model, particles are treated as continuum and the effect of discreteness or the correlation between particle positions is completely neglected. The above result indicates that we have to take into account the effect of discreteness: Correlations between particles reduce the interaction energy and may lead to reduced thickness.

### 4.2 Sheet Model without Cohesive Energy

The effect of discreteness appears as the formation of layers penpendicular to the $z$-axis and the formation of lattice structures in each layer. Let us here assume that our system is composed of thin planar sheets and take the first effect of discreteness into account. Suppose we have $\mathcal{N}$ thin planar sheets of surface number densities $n_i$ at $z = z_i$, $i = 1, 2, \ldots \mathcal{N}$, and

$$N_s = \sum_i n_i. \tag{44}$$

When we neglect the correlation of particle positions in each sheet and assume that particles are distributed uniformly, the interaction energy of our system is given by

$$\begin{aligned} &\frac{1}{2}\int\int d\mathbf{r}d\mathbf{r}' \sum_{ij} n_i n_j \delta(z - z_i)\delta(z' - z_j)\frac{q^2}{|\mathbf{r} - \mathbf{r}'|}\exp(-\kappa|\mathbf{r} - \mathbf{r}'|) \\ = \; & N_s \int d\mathbf{R}\frac{\pi}{N_s}\frac{q^2}{\kappa}\sum_{ij} n_i n_j \exp(-\kappa|z_i - z_j|). \end{aligned} \tag{45}$$

In comparison with the uniform distribution with the thickness $2d$, the interaction energy (per particle) in the state of uniform sheets is given by

$$\Delta U = \frac{\pi}{N_s}\frac{q^2}{\kappa}\sum_{ij} n_i n_j \exp(-\kappa|z_i - z_j|) - \frac{\pi}{2}\frac{q^2 N_s}{\kappa^3 d^2}[\exp(-2\kappa d) - 1 + 2\kappa d]. \tag{46}$$

When $\kappa = 0$, (46) reduces to

$$\Delta U_{\kappa=0} = -\frac{\pi}{N_s}q^2\sum_{ij} n_i n_j |z_i - z_j| + \frac{2\pi}{3}q^2 N_s d. \tag{47}$$

When we have two sheets of the surface density $n/2$ at $z = \pm L$, (47) gives

$$\Delta U_1 = -\pi q^2 N_s L + \frac{2\pi}{3}q^2 N_s d. \tag{48}$$

In (3.4) of previous analysis,[10] the zero of the potential has been taken at $U_1$.

In a one-dimensional potential $kz^2/2$ the total potential energy per particle is given by

$$\frac{1}{2}\sum_i \frac{n_i}{N_s}kz_i^2 + \frac{\pi}{N_s}\frac{q^2}{\kappa}\sum_{ij} n_i n_j \exp(-\kappa|z_i - z_j|). \tag{49}$$

When we minimize the potential energy with respect to $n_i$, $z_i$, and $\mathcal{N}$ for given values of $N_s$, we have the result shown in Figs. 8 and 9. When the number of sheets is appropriately assumed, experimental results of thickness are approximately reproduced. The minimum energy state, however, is given by the state of infinite sheets as in the case of OCP.[9]

### 4.3 Sheet Model with Cohesive Energy

We have seen that, when our system is composed of uniform sheets, the state of the lowest energy is realized by infinite number of sheets. In the above analysis, only the effect of discreteness in $z$-direction is taken into account by assuming the existence of sheets. Since the effect of discreteness in the $xy$-plane leads to a negative cohesive energy in each sheet, we have a possibility to stabilize the state of finite number of sheets by including the cohesive energy within each sheet: We have a

tradeoff between inter-sheet interaction energy and intra-sheet cohesive energy which has smaller value for larger density in each sheet and favors smaller number of sheets.

The cohesive energy may be defined as the difference between the interaction energy per particle with correlation and that of uniform distribution. As is shown in Appendix B, the cohesive energy in each sheet per particle for a sheet of the surface density $n_i$ is expressed by a function of $\kappa n_i^{-1/2}$ as

$$q^2 n_i^{1/2} e_{coh}(\kappa n_i^{-1/2}). \tag{50}$$

In the limit of $\kappa = 0$, $e_{coh}(\kappa n_i^{-1/2})$ reduces to the values for the two-dimensional OCP.[19] Values of $e_{coh}(\kappa n_i^{-1/2})$ are computed for the triangular and square lattices and are shown in Fig. 10.

The total potential energy is given by

$$\frac{1}{2}\sum_i \frac{n_i}{N_s} k z_i^2 + \frac{\pi}{N_s}\frac{q^2}{\kappa}\sum_{ij} n_i n_j \exp(-\kappa|z_i - z_j|) + \sum_i \frac{n_i}{N_s} q^2 n_i^{1/2} e_{coh}(\kappa n_i^{-1/2}). \tag{51}$$

When we minimize the above expression with respect to all parameters for given $N_s$ and $k$, we have the results shown in Fig. 11 and thick lines in Figs. 2 and 3.

Our continuum model gives the thickness as much as twice the experimental results. When the effect of discreteness is taken into account by considering the formation of sheets, theoretical thickness becomes comparable with experimental ones. In this case, however, the state with larger number of sheetes gives lower energy. The last point is improved by the inclusion of the effect of discreteness in each sheet through the cohesive energy of two-dimensional Yukawa system and we are able to reproduce the transitions in the number of layers observed in numerical experiments.

## 5 CONCLUDING REMARKS

Dusty plasmas are modeled by a Yukawa system composed of particles of one species in a one-dimensional parabolic potential and numerical simulations have been performed. It has been shown that particles form thin layers at low temperatures and discrete transitions in the number of layers have been observed. Extending the theoretical model which has been successful for confined OCP's, we have developed a theory for Yukawa system in external potentials and reproduced the number, the positions, and populations of layers to a good accuracy.

We have systems of particles which are regarded as dusty plasmas in a variety of situations including plasma processes for semiconductor engineering and plasmas in space. Our results for simplified Yukawa system may be useful to estimate parameters such as the density and external force fields and control the behavior of dusty plasmas.

## ACKNOWLEDGEMENTS

This work has been partly supported by the Grants-in-Aid for Scientific Research from the Ministry of Education, Science, Sports, and Culture of Japan, Nos.06680448 and 08458109.

## APPENDIX A Two-Dimensional Yukawa Lattice Sum

We rewrite the Yukawa potential into the form

$$\frac{q^2}{r}\exp(-\kappa r) = \frac{2}{\sqrt{\pi}}q^2\left(\int_0^G + \int_G^\infty\right)dt\exp\left(-r^2t^2 - \frac{\kappa^2}{4t^2}\right) \tag{52}$$

and Fourier-transform the long-range part of the lattice sum. For Yukawa system with two-dimensional periodicity $\{\mathbf{P} = n_1\mathbf{a} + n_2\mathbf{b}\}$, we have

$$\begin{aligned}
&\sum_{\mathbf{P}}\frac{1}{|\mathbf{P}-\mathbf{r}|}\exp\left(-\kappa|\mathbf{P}-\mathbf{r}|\right) \\
&= \frac{1}{2}\sum_{\mathbf{P}}\frac{1}{|\mathbf{P}-\mathbf{r}|}\left[\exp\left(\kappa|\mathbf{P}-\mathbf{r}|\right)\mathrm{erfc}\left(G|\mathbf{P}-\mathbf{r}| + \frac{\kappa}{2G}\right) + \exp\left(-\kappa|\mathbf{P}-\mathbf{r}|\right)\mathrm{erfc}\left(G|\mathbf{P}-\mathbf{r}| - \frac{\kappa}{2G}\right)\right] \\
&\quad + \frac{\pi}{S_0}\sum_{\mathbf{K}}\frac{1}{\sqrt{K^2+\kappa^2}}\exp(i\mathbf{K}\cdot\mathbf{R}) \\
&\quad \times\left[\exp(\sqrt{K^2+\kappa^2}z)\mathrm{erfc}\left(\frac{\sqrt{K^2+\kappa^2}}{2G} + Gz\right) + \exp(-\sqrt{K^2+\kappa^2}z)\mathrm{erfc}\left(\frac{\sqrt{K^2+\kappa^2}}{2G} - Gz\right)\right]
\end{aligned} \tag{53}$$

Here $\{\mathbf{K}\}$ is the reciprocal lattice of $\{\mathbf{P}\}$ and $S_0$ is the area of the unit cell in two dimensions. The interaction energy between a particle and its own image $\phi_0$ (the Madelung energy of two-dimensional lattice $\{\mathbf{P}\}$) is given by

$$\begin{aligned}
\frac{\phi_0}{q^2} &= \lim_{r\to 0}\left[\sum_{\mathbf{P}}\frac{1}{|\mathbf{P}-\mathbf{r}|}\exp\left(-\kappa|\mathbf{P}-\mathbf{r}|\right) - \frac{1}{r}\exp(-\kappa r)\right] \\
&= \frac{1}{2}\sum_{\mathbf{P}\neq 0}\frac{1}{P}\left[\exp(\kappa P)\mathrm{erfc}\left(GP + \frac{\kappa}{2G}\right) + \exp(-\kappa P)\mathrm{erfc}\left(GP - \frac{\kappa}{2G}\right)\right] \\
&\quad + \frac{2\pi}{S_0}\sum_{\mathbf{K}}\frac{1}{\sqrt{K^2+\kappa^2}}\mathrm{erfc}\left(\frac{\sqrt{K^2+\kappa^2}}{2G}\right) + \kappa\,\mathrm{erfc}\left(\frac{\kappa}{2G}\right) - \frac{2}{\sqrt{\pi}}G\exp\left(-\frac{\kappa^2}{4G^2}\right).
\end{aligned} \tag{54}$$

For a system with two-dimensional periodicity $\{\mathbf{P}\}$ in the $xy$ plane, $\Pi$ is given by

$$\Pi = -\frac{1}{2S_0}\sum_{i\neq j}\sum_{\mathbf{P}}\frac{(\mathbf{R}_{ij}-\mathbf{P})(\mathbf{R}_{ij}-\mathbf{P})}{|\mathbf{r}_{ij}-\mathbf{P}|}\frac{\partial}{\partial|\mathbf{r}_{ij}-\mathbf{P}|}v\left(|\mathbf{r}_{ij}-\mathbf{P}|\right) - \frac{N}{2S_0}\sum_{\mathbf{P}\neq 0}\frac{\mathbf{P}\mathbf{P}}{P}\frac{\partial}{\partial P}v(P), \tag{55}$$

where $\mathbf{r}_{ij} = \mathbf{r}_i - \mathbf{r}_j$ and $\mathbf{R}_{ij} = \mathbf{R}_i - \mathbf{R}_j$. The first and the second lattice sums on the right-hand side are calculated by the Ewald method as follows.

For Yukawa system with two-dimensional periodicity $\{\mathbf{P}\}$ we have

$$\begin{aligned}
&\sum_{\mathbf{P}}\frac{(\mathbf{r}-\mathbf{P})(\mathbf{r}-\mathbf{P})}{|\mathbf{r}-\mathbf{P}|}\left\{\frac{\partial}{\partial|\mathbf{r}-\mathbf{P}|}\frac{1}{|\mathbf{r}-\mathbf{P}|}\exp\left(-\kappa|\mathbf{r}-\mathbf{P}|\right)\right\} \\
&= -\sum_{\mathbf{P}}\frac{(\mathbf{r}-\mathbf{P})(\mathbf{r}-\mathbf{P})}{|\mathbf{r}-\mathbf{P}|^3}\left\{\frac{1}{2}\left(1-\kappa|\mathbf{r}-\mathbf{P}|\right)\exp\left(\kappa|\mathbf{r}-\mathbf{P}|\right)\mathrm{erfc}\left(G|\mathbf{r}-\mathbf{P}| + \frac{\kappa}{2G}\right)\right. \\
&\quad + \frac{1}{2}\left(1+\kappa|\mathbf{r}-\mathbf{P}|\right)\exp\left(-\kappa|\mathbf{r}-\mathbf{P}|\right)\mathrm{erfc}\left(G|\mathbf{r}-\mathbf{P}| - \frac{\kappa}{2G}\right) \\
&\quad \left. + \frac{2}{\sqrt{\pi}}G|\mathbf{r}-\mathbf{P}|\exp\left(-G^2|\mathbf{r}-\mathbf{P}|^2 - \frac{\kappa^2}{4G^2}\right)\right\}
\end{aligned}$$

$$+\frac{1}{S_0}\sum_{\mathbf{K}}\frac{1}{2\pi}\int_{-\infty}^{\infty}dg_z\mathbf{gg}\frac{8\pi}{(g^2+\kappa^2)^2}\left(\frac{g^2+\kappa^2}{4G^2}+1\right)\exp\left(-\frac{g^2+\kappa^2}{4G^2}+i\mathbf{g}\cdot\mathbf{r}\right)$$
$$-1\frac{1}{S_0}\sum_{\mathbf{K}}\frac{1}{2\pi}\int_{-\infty}^{\infty}dg_z\frac{4\pi}{g^2+\kappa^2}\exp\left(-\frac{g^2+\kappa^2}{4G^2}+i\mathbf{g}\cdot\mathbf{r}\right), \tag{56}$$

where

$$\mathbf{g}=\mathbf{K}+g_z\hat{z}\quad\text{and}\quad\mathbf{gg}=\mathbf{KK}+\mathbf{K}g_z\hat{z}+g_z\hat{z}\mathbf{K}+g_z^2\hat{z}\hat{z}. \tag{57}$$

The first term on the right-hand side of (55) is given by the $2\times 2$ part of the above tensor as

$$\sum_{\mathbf{P}}\frac{(\mathbf{R}-\mathbf{P})(\mathbf{R}-\mathbf{P})}{|\mathbf{r}-\mathbf{P}|}\left\{\frac{\partial}{\partial|\mathbf{r}-\mathbf{P}|}\frac{1}{|\mathbf{r}-\mathbf{P}|}\exp\left(-\kappa|\mathbf{r}-\mathbf{P}|\right)\right\}$$
$$=-\sum_{\mathbf{P}}\frac{(\mathbf{R}-\mathbf{P})(\mathbf{R}-\mathbf{P})}{|\mathbf{r}-\mathbf{P}|^3}\left\{\frac{1}{2}(1-\kappa|\mathbf{r}-\mathbf{P}|)\exp\left(\kappa|\mathbf{r}-\mathbf{P}|\right)\mathrm{erfc}\left(G|\mathbf{r}-\mathbf{P}|+\frac{\kappa}{2G}\right)\right.$$
$$+\frac{1}{2}(1+\kappa|\mathbf{r}-\mathbf{P}|)\exp\left(-\kappa|\mathbf{r}-\mathbf{P}|\right)\mathrm{erfc}\left(G|\mathbf{r}-\mathbf{P}|-\frac{\kappa}{2G}\right)$$
$$\left.+\frac{2}{\sqrt{\pi}}G|\mathbf{r}-\mathbf{P}|\exp\left(-G^2|\mathbf{r}-\mathbf{P}|^2-\frac{\kappa^2}{4G^2}\right)\right\}$$
$$+\frac{1}{S_0}\sum_{\mathbf{K}}\frac{1}{2\pi}\int_{-\infty}^{\infty}dg_z\mathbf{KK}\frac{8\pi}{(g^2+\kappa^2)^2}\left(\frac{g^2+\kappa^2}{4G^2}+1\right)\exp\left(-\frac{g^2+\kappa^2}{4G^2}+i\mathbf{g}\cdot\mathbf{r}\right)$$
$$-1\frac{1}{S_0}\sum_{\mathbf{K}}\frac{1}{2\pi}\int_{-\infty}^{\infty}dg_z\frac{4\pi}{g^2+\kappa^2}\exp\left(-\frac{g^2+\kappa^2}{4G^2}+i\mathbf{g}\cdot\mathbf{r}\right). \tag{58}$$

Integrations with respect to $g_z$ give

$$\frac{1}{S_0}\sum_{\mathbf{K}}\frac{1}{2\pi}\int_{-\infty}^{\infty}dg_z\frac{4\pi}{g^2+\kappa^2}\exp\left(-\frac{g^2+\kappa^2}{4G^2}+i\mathbf{g}\cdot\mathbf{r}\right)$$
$$=\frac{1}{S_0}\sum_{\mathbf{K}}\frac{\pi}{\sqrt{K^2+\kappa^2}}\exp(i\mathbf{K}\cdot\mathbf{R})\times\left[\exp(\sqrt{K^2+\kappa^2}|z|)\mathrm{erfc}(\frac{\sqrt{K^2+\kappa^2}}{2G}+G|z|)\right.$$
$$\left.+\exp(-\sqrt{K^2+\kappa^2}|z|)\mathrm{erfc}(\frac{\sqrt{K^2+\kappa^2}}{2G}-G|z|)\right], \tag{59}$$

and

$$\frac{1}{S_0}\sum_{\mathbf{K}}\frac{1}{2\pi}\int_{-\infty}^{\infty}dg_z\frac{8\pi}{(g^2+\kappa^2)^2}\left(\frac{g^2+\kappa^2}{4G^2}+1\right)\exp\left(-\frac{g^2+\kappa^2}{4G^2}+i\mathbf{g}\cdot\mathbf{r}\right)$$
$$=\frac{\pi}{S_0}\sum_{\mathbf{K}}\frac{\exp(i\mathbf{K}\cdot\mathbf{R})}{(K^2+\kappa^2)^{3/2}}\left[(1-\sqrt{K^2+\kappa^2}|z|)\exp(\sqrt{K^2+\kappa^2}|z|)\mathrm{erfc}(\frac{\sqrt{K^2+\kappa^2}}{2G}+G|z|)\right.$$
$$+(1+\sqrt{K^2+\kappa^2}|z|)\exp(-\sqrt{K^2+\kappa^2}|z|)\mathrm{erfc}(\frac{\sqrt{K^2+\kappa^2}}{2G}-G|z|)$$
$$\left.+\frac{2}{\sqrt{\pi}}\frac{\sqrt{K^2+\kappa^2}}{G}\exp(-\frac{K^2+\kappa^2}{4G^2}-G^2z^2)\right]. \tag{60}$$

The second term on the right-hand side of (55) is similarly calculated as

$$\sum_{\mathbf{P}\neq\mathbf{0}}\frac{\mathbf{PP}}{P}\frac{\partial}{\partial P}\frac{1}{P}\exp(-\kappa P)$$

$$
\begin{aligned}
= & -\sum_{\mathbf{P}\neq\mathbf{0}} \frac{\mathbf{PP}}{P^3}\left\{\frac{1}{2}(1-\kappa P)\exp(\kappa P)\mathrm{erfc}\left(GP+\frac{\kappa}{2G}\right)\right. \\
& \left.+\frac{1}{2}(1+\kappa P)\exp(-\kappa P)\mathrm{erfc}\left(GP-\frac{\kappa}{2G}\right)+\frac{2}{\sqrt{\pi}}GP\exp\left(-G^2P^2-\frac{\kappa^2}{4G^2}\right)\right\} \\
& +\frac{1}{S_0}\sum_{\mathbf{K}}\frac{1}{2\pi}\int_{-\infty}^{\infty}dg_z\mathbf{KK}\frac{8\pi}{(g^2+\kappa^2)^2}\left(\frac{g^2+\kappa^2}{4G^2}+1\right)\exp\left(-\frac{g^2+\kappa^2}{4G^2}\right) \\
& -1\frac{1}{S_0}\sum_{\mathbf{K}}\frac{1}{2\pi}\int_{-\infty}^{\infty}dg_z\frac{4\pi}{g^2+\kappa^2}\exp\left(-\frac{g^2+\kappa^2}{4G^2}\right). \qquad (61)
\end{aligned}
$$

## APPENDIX B Cohesive Energy of Two-Dimensional Yukawa Lattice

When particles are distributed uniformly in a plane with the surface number density $n$, the interaction energy per particle is given by

$$\frac{1}{2}n\int d\mathbf{R}\frac{q^2}{R}\exp(-\kappa R)=\pi\frac{n}{\kappa}q^2, \qquad (62)$$

$\mathbf{R}$ being the two-dimensional coordinates in the plane. In this case, there is no correlation between positions of particles.

The effect of correlation reduces the interaction energy. The cohesive energy of a lattice $\{\mathbf{P}\}$ is given by the difference between the Madelung energy $\phi_0$ and (62) as

$$E_{coh}=\frac{\phi_0}{2}-\frac{\pi}{S_0\kappa}q^2. \qquad (63)$$

Here we have noted that $n=1/S_0$. We note that when $\kappa=0$ the expression (63) reduces to the case of the two-dimensional one-component plasma.[19]

The cohesive energy may be expressed by a nondimensional function of $\kappa n^{-1/2}$, $e_{coh}(\kappa n^{-1/2})$, as

$$E_{coh}=q^2n^{1/2}e_{coh}(\kappa n^{-1/2}). \qquad (64)$$

In the case of OCP or $\kappa=0$, we have $e_{coh}(\kappa n^{-1/2}=0)\sim -1.9605158$ for the triangular lattice and $\sim -1.9501325$ for the square lattice.[19] Values of $e_{coh}(\kappa n^{-1/2})$ are computed by (54) for the triangular and square lattices.

Noting that the absolute value of $e_{coh}(\kappa n^{-1/2})$ decreases exponentially for large values of $\kappa n^{-1/2}$, we interpolate the values of $e_{coh}(\kappa n^{-1/2})$ by

$$e_{coh}(x)=-\exp(0.6732-0.02530x)\quad 0\le x\le 3 \text{ (triangular lattice)} \qquad (65)$$

and

$$e_{coh}(x)=-\exp(0.6679-0.02536x)\quad 0\le x\le 3 \text{ (square lattice)} \qquad (66)$$

The relative error of this expression is less than 1%. We use this interpolation in the computations in Section 4.

## REFERENCES

[1] H. Thomas, G. E. Morfill, V. Demmel, J. Goree, B. Feuerbacher, and D. Möhlmann, Phys. Rev. Lett. **73**, 652(1994).

[2] J. H. Chu and Lin I, Physica A **205**(1994)183 : Phys. Rev. Lett. **72**, 4009(1994).

[3] Y. Hayashi and T. Tachibana, Jpn. J. Appl. Phys. **33**, L804(1994).

[4] A. Melzer, T. Trottenberg, and A.Piel, Phys. Lett. A **191**, 301(1994).

[5] For example, H. M. Thomas and G. E. Morfill, Nature **379**, 806(1996).

[6] Some earlier results are given in H. Totsuji, T. Kishimoto, Y. Inoue, C. Totsuji, and S. Nara, Physics Letters A **221**, 215(1996).

[7] H. Ikezi, Phys. Fluids **29**, 1764(1986).

[8] For example, M. O. Robbins, K. Kremer, and G. S. Grest, J. Chem. Phys. **88**, 3286(1988).

[9] H. Totsuji and J. -L. Barrat, Phys. Rev. Lett. **60**, 2484(1988).

[10] H. Totsuji, *Strongly Coupled Plasma Physics* (ed. S. Ichimaru, Elsevier Science Publishers, 1990), p. 213.

[11] H. Totsuji, H. Shirokoshi, and S. Nara, Phys. Lett. A **162**, 174(1992).

[12] M. Parrinello and A. Rahman, Phys. Rev. Lett. **45**, 1196(1980); M. Parrinello, A. Rahman, and P. Vashishta, Phys. Rev. Lett. **50**, 1073(1983).

[13] S. Nosé, J. Chem. Phys. **81**, 511(1984).

[14] H. C. Anderson, J. Chem. Phys. **72**, 2384(1980).

[15] J. P. Schiffer, Phys. Rev. Lett. **61**, 1843(1988).

[16] J. P. Schiffer, Phys. Rev. Lett. **70**, 818(1993).

[17] D. H. E. Dubin, Phys. Rev. Lett. **71**, 2753(1993).

[18] D. H. Van Winkle and C. A. Murray, Phys. Rev. A **34**, 562(1986).

[19] H. Totsuji, Phys. Rev. A **17**, 399(1978).